remote sensing

Article

Absolute Radiometric Calibration of an Imaging Spectroradiometer Using a Laboratory Detector-Based Approach

Zhipeng Wang [1,*], Kurtis Thome [2], Ronald Lockwood [3] and Brian N. Wenny [1]

1 Science Systems and Applications, Inc., Lanham, MD 20706, USA; brian.n.wenny@nasa.gov
2 Sciences and Exploration Directorate, Goddard Space Flight Center, NASA, Greenbelt, MD 20771, USA; kurtis.thome@nasa.gov
3 Lincoln Laboratory, Massachusetts Institute of Technology (MIT), Lexington, MA 02421, USA; ronald.lockwood@ll.mit.edu
* Correspondence: zhipeng.wang@nasa.gov

Abstract: The HyperSpectral Imager for Climate Science (HySICS) is the core instrument of the Climate Absolute Refractivity and Reflectance Observatory (CLARREO) Pathfinder (CPF) mission and is currently scheduled to be launched to the International Space Station (ISS) in 2023. HySICS is an Offner–Chrisp imaging spectrometer designed to meet an unprecedented radiometric uncertainty requirement of 0.3% ($k = 1$) over its entire spectral range of 350–2300 nm. The approach represents the need for significant improvement over the Radiometric Calibration (RadCal) of existing space-borne spectrometers. One strategy to demonstrate that HySICS achieves this level of accuracy is through an Independent Calibration (IndCal) effort that can provide an alternative referencing RadCal, which follows a traceability chain independent of the operational RadCal of ratioing approach. The IndCal relies on a pre-launch detector-based absolute RadCal of HySICS, using a tunable laser system as source, and the system planned for the HySICS absolute RadCal is the Goddard Laser for Absolute Measurement of Radiance (GLAMR). GLAMR was developed at NASA's Goddard Space Flight Center and has been used to calibrate multiple operational remote sensing instruments, as well as the SOlar, Lunar Absolute Reflectance Imaging Spectroradiometer (SOLARIS), a calibration demonstration system developed for the CLARREO mission. In this work, the data of SOLARIS GLAMR RadCal conducted in 2019 are processed to derive the Absolute Spectral Response (ASR) functions and other key characterization parameters of SOLARIS detectors. The results are further analyzed with the goals to plan the HySICS GLAMR RadCal, in particular to optimize its configuration, to demonstrate the traceability route to the NIST standard, and to develop the error budget of the calibration approach. The SOLARIS calibration is also compared with other source- and detector-based calibrations to validate the absolute radiometric accuracy achieved.

Keywords: radiometric calibration; hyperspectral sensor; traceability; error budget; sensor design

check for updates

Citation: Wang, Z.; Thome, K.; Lockwood, R.; Wenny, B.N. Absolute Radiometric Calibration of an Imaging Spectroradiometer Using a Laboratory Detector-Based Approach. *Remote Sens.* **2022**, *14*, 2245. https://doi.org/10.3390/rs14092245

Academic Editor: Charles M. Bachmann

Received: 27 February 2022
Accepted: 4 May 2022
Published: 7 May 2022

1. Introduction

The increasing availability of space-borne remote sensing instruments for climate monitoring, weather forecasting, and miscellaneous environmental applications has grown in parallel with the development of on-orbit Radiometric Calibration (RadCal) techniques that accurately convert the sensor response to at-sensor spectral radiance. The stability of the sensor's RadCal tends to be much better than the absolute accuracy, so instrument stability is typically specified to be significantly smaller than that for absolute uncertainty. For example, values for the Visible and Infrared Imaging Radiometer Suite (VIIRS) are 0.3% ($k = 1$) and 2% ($k = 1$), respectively, for stability versus absolute uncertainty [1]. The development of long-term climate records requires a combination of measurements from multiple satellite sensors either as part of a single series, such as various Landsat sensors from 1972 to the present [2]; overlapping identical sensors on multiple platforms such as the Moderate Resolution Imaging Spectroradiometer (MODIS) on the Terra (since 1999) and Aqua (since 2002) platforms; or multiple sensors across multiple platforms, as is the case for MODIS being followed on by VIIRS on the S-NPP/Joint Polar Satellite System (JPSS) series since 2011 [3,4]. The stability of the RadCal of an individual sensor is still important, but absolute calibration accuracy becomes critical to ensure consistency among the data records across the sensors. The absolute RadCal strategy has continuously evolved in response to such needs by the science community, as well as the development of sensors with high SI-traceable RadCal accuracy to serve as an on-orbit inter-calibration reference for other orbiting sensors.

Studies undertaken as part of the Climate Absolute Radiance and Refractivity Observatory (CLARREO) mission recognized the importance of the traceability to the International System of Units (SI), as well as for very high absolute accuracy for climate quality data sets. The work shows that an absolute uncertainty requirement of 0.3% (k = 2) is needed in the reflected solar spectrum in order to observe climate change to within the uncertainty of natural variability [5]. The requirement of radiometric accuracy for the CLARREO Reflective Solar (RS) spectrometer is defined accordingly. The current version of the mission, CLARREO Pathfinder (CPF) from the National Aeronautics and Space Administration (NASA) [6], and similarly, TRUTHS from the European Space Agency (ESA) [7] are planned to provide precise measurements of key climate variables at the designated accuracy. They are also projected to serve as the SI-traceable (i.e., metrologically traceable to SI) on-orbit references to inter-calibrate other remote sensing instruments [8]. The core instrument of the CPF mission is the HyperSpectral Imager for Climate Science (HySICS), to be launched to the International Space Station (ISS) in 2023 [9]. HySICS is an Offner–Chrisp imaging spectrometer designed to meet a radiometric uncertainty requirement of 0.3% (k = 1) over its entire spectral range of 350–2300 nm. An absolute RadCal strategy with the capability to reach this level of accuracy, which is a significant improvement over the RadCal of previous space-borne spectrometers, needs to be developed and incorporated.

A technique developed at the National Institute of Standards and Technology (NIST) makes use of wavelength-tunable lasers coupled to a Spherical Integrating Source (SIS) and relies on detector-based methods for SI-traceability to meet the high accuracy requirement [10]. The main advantage offered by the laser-based approach over the conventional lamp-illuminated SIS approach is the use of a high-power, near-monochromatic source that eliminates the need for using a spectral filter, the largest source of uncertainty during pre-launch RadCal. The approach also allows the sensor's entrance pupil to be uniformly filled, allowing for the full sensor spatial and spectral characteristics to be evaluated as the source is tuned across the spectral response range of the sensor. In addition, the laser-based sources offer opportunities for high-radiance source values and thus a high signal-to-noise ratio (SNR), which is necessary to characterize detectors at low responsivity, such as the Day–Night Band (DNB) of VIIRS.

An implementation of the above NIST approach was undertaken as part of the CLARREO project leading to the Goddard Laser for Absolute Measurement of Radiance (GLAMR) developed at the NASA Goddard Space Flight Center (GSFC). GLAMR has been successfully used to characterize the radiometric and spectral responses of JPSS-2, 3, and 4 VIIRS, as well as the Landsat-8 Operational Land Imager (OLI) and Landsat-9 OLI-2 [11–13]. These results relied primarily on the relative spectral response capabilities of GLAMR, while the absolute RadCal has been demonstrated with the calibration of an airborne imaging spectrometer [14]. The GLAMR work planned for CPF will be the first instance of using GLAMR for the detector-based absolute RadCal of a satellite-based sensor.

The strategy to demonstrate that HySICS achieves this level of uncertainty includes an independent calibration effort through a pre-launch, detector-based RadCal using GLAMR. The SOlar, Lunar Absolute Reflectance Imaging Spectroradiometer (SOLARIS) developed as a calibration demonstration system for the CLARREO mission is used to verify GLAMR's methodology and operational readiness for use with HySICS. The work with SOLARIS also provides the means to evaluate the processing approach to derive a broadband radiometric calibration suitable for use with solar-illuminated scenes. This paper reports the methodology and results of a SOLARIS absolute RadCal. Results from the GLAMR-based testing indicate that the uncertainty across the SOLARIS spectrum is <0.6% (k = 2) in spectral regions for which the GLAMR source maintains stability and the SOLARIS SNR exceeds 200 for the in-band response peak. The independent calibration of HySICS using GLAMR provides an added traceability path to validate and improve the credibility of CPF's absolute and relative uncertainty budgets.

The paper is organized as follows: Section 2 describes the methodology of detector-based calibration and its recent realization at NASA GSFC with GLAMR as light source. It is followed by a description of SOLARIS instrument and its GLAMR-based absolute RadCal in Section 3. Section 4 presents the data processing methodology and results of the calibration, including the derivation of key radiometric parameters for SOLARIS. An uncertainty budget analysis showing that the current uncertainty levels are sufficient to achieve the 0.3% (k = 1) requirements of CPF is provided in Section 5. Comparisons of GLAMR-based calibrations using a non-imaging, multispectral radiometer to those from more traditional source-based approaches are also included in Section 5 to demonstrate that the assessed uncertainties are reasonable. The discussion and conclusions in Section 6 include a description of how the lessons learned from the SOLARIS work can be applied to the more general imaging spectrometer case, including that of HySICS, as guidance for sampling and collection approaches for absolute radiometric calibration of imaging spectrometers.

2. Detector-Based Calibration with a Tunable Laser Source

2.1. Detector-Based Calibration Approach

In principal, the RadCal of satellite imaging systems refers to the ability to convert the digital numbers recorded by the instrument into physical units. The RadCal process makes use of calibration sources with outputs of a known physical quantity, such as optical power, to illuminate the sensor under test, providing the relationship between the sensor output units to the calibration source physical units. The calibration standards can be viewed as transfer standards in that they provide a transfer of the values of the primary standard, which is a device used as the calibration reference that is acknowledged to be of the highest metrological quality without referencing to some other standard of the same quantity [15], to the calibration laboratory standard for subsequent transfer to a device under test. Traceable calibrations have an unbroken chain of transfer comparisons that are certified to be traceable back to the national primary standard. Calibration uncertainty is then dependent on the calibration hierarchy from the standard to the sensor under test. Since the calibration transfer is a real hardware transfer of the standard itself, careful handling and operation of the calibration standard is extremely important. RadCal is the most important prerequisite for accuracy in measurement instrumentation [16,17].

There are two possible ways to perform an absolute radiometric calibration: source-based and detector-based. The source-based method is the traditional approach and relies on a source being calibrated with a known traceability to the necessary physical units. The calibration laboratory uses this source directly in the calibration of the sensor under test or as the standard used to calibrate the source used in the sensor calibration. The calibration equation is built between the source's output and the sensor's output. The key assumption in a source-based method is that the output of the reference source does not change with time. The detector-based calibrations still rely on a source in the calibration laboratory being calibrated with known traceability to the necessary physical units. The key difference is that the calibration laboratory source is calibrated using a calibrated detector package. The calibration equation is built between the calibrated detector's output and the sensor's output. The detector-based method makes the assumption that the detector package does not change with time and that the package maintains traceability if the detector package makes use of the same measurement geometry.

One way to view the difference is that in a source-based method, the source is calibrated and then transported to the user's calibration facility, while in the detector-based approach, it is the detector package that is calibrated and sent to the user. Due to the high levels of maintenance and care required to operate optical radiation sources, detector-based standards are very attractive alternatives. The detectors, in particular semiconductor detectors, have the advantage of long-term absolute and mechanical stability.

2.2. Tunable Laser Source: GLAMR

The key to the accuracy of detector-based methods is the use of high-accuracy reference detectors, or transfer radiometers (TRs), and their high accuracy is an outcome of not including any spectral filter. Using such radiometers necessitates the use of narrow spectral sources to prevent detector saturation. If a detector's spectral responsivity is to be measured over its entire active bandpass, the creation of monochromatic radiation at all of the different required wavelengths is required. Thus, tunable lasers are ideal in the calibration system to provide a narrow-band source that allows the TRs to be operated without spectral filters.

The near-monochromatic characteristic of such a source is also the key to quantifying stray light in the instrument under test since it simplifies the complexity of the source beam. The negative aspect of using narrow spectral sources is that they do not match the broadband spectral nature of the sources used in terrestrial remote sensing. In addition, the complexity of determining a band-averaged radiometric calibration for imaging spectrometers from the monochromatic approach is more complicated than that employed by broadband approaches. The complexities of the detector-based method are outweighed by the improved absolute accuracy; thus, it becomes important to show that the results of tunable source calibration are suitable for broadband source applications.

The use of a tunable laser source for detector-based absolute RadCal meeting the CPF requirements was first demonstrated by NIST with Spectral Irradiance and Radiance responsivity Calibrations using Uniform Sources (SIRCUS) [18]. Calibration scientists at NASA GSFC developed the GLAMR system based on a traveling version of SIRCUS (T-SIRCUS). The configuration of GLAMR used for the SOLARIS calibration in this work includes several laser sources that cover the full spectral range from 350 to 2500 nm. The basic concept is that a pump laser operating at its output wavelength is used with an Optical Parametric Oscillator (OPO) to produce output energy at a range of wavelengths. Most of the spectral range is accessed using a custom-built OPO and its harmonics. This oscillator is pumped by a 532 nm, picosecond pulse, mode-locked laser with an 80 MHz repetition rate and a temperature-phase-matched Lithium Triborate (LBO) crystal for parametric oscillation in a ring cavity. For the OPO NIR beam path, the OPO fundamental tuning range is 680 nm to 1100 nm and 340 nm to 550 nm in the second harmonic. In addition, the mirrors become partially transmissive to the idler wavelength at 1200 nm, so the idler output of the OPO from 1200 nm to 2200 nm can also be used. A separate OPO SWIR beam path provides a tuning capacity from 1100 nm to 1200 nm and 550 nm to 770 nm in the second harmonic. Two commercial lasers, the ARGOS by Aculight Corp. and the CLT by IPG Photonics Corp., each sit on their own bench and provide complete redundancy for wavelengths above 2200 nm [12,19]. Figure 1 summarizes the sources used to cover the spectral CPF independent calibration range of SOLARIS for calibrations. The spectral ranges are also separately listed in Table 1.

GLAMR has been used to characterize the radiometric and spectral response of multiple milestone remote sensing instruments such as VIIRS and Landsat OLI. Figure 2 shows the radiance of GLAMR measured during a recent VIIRS RadCal. The radiance from GLAMR is stabilized over short periods using a feedback monitor, which is in the integrating sphere to control a set of crossed polarizers. The design allows the output to be adjusted to various radiance levels, providing the flexibility of calibrating instrument detectors over a large dynamic range. The data in Figure 2 show the spectral radiance levels that were provided for both in-band and out-of-band characterizations, as well as multiple radiance levels for bands with similar bandpasses, but different gain levels.

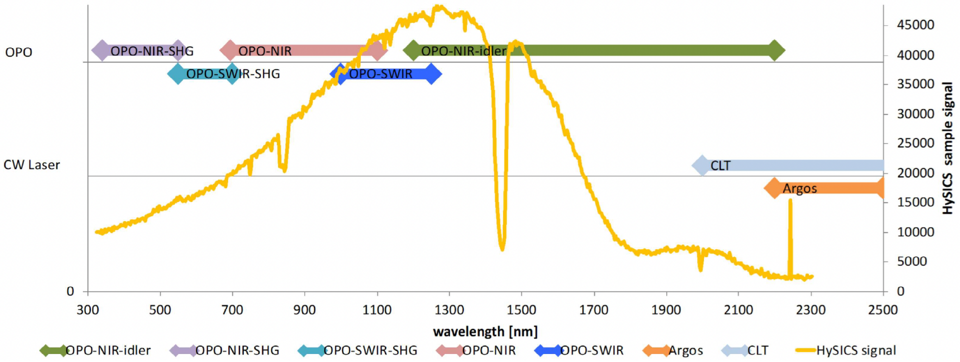

Figure 1. The spectral coverage of GLAMR with its several tunable laser sources.

Table 1. Spectral coverage of GLAMR lasers.

Laser Type	Wavelength Range (nm)
OPO_NIR_SHG	385–550
OPO_SWIR_SHG	550–700
OPO_NIR	700–1100
OPO_SWIR	1100–1200
OPO_NIR_Idler	1200–2200
CLT	2000–2500
ARGOS	2185–2500

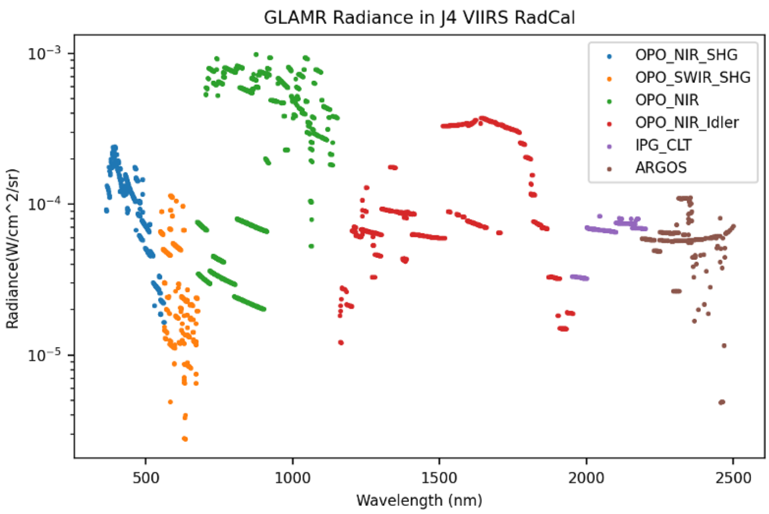

Figure 2. The GLAMR radiance measured during the JPSS-4 VIIRS RadCal. Each data point is the mean radiance at a wavelength step.

2.3. SI Traceability of GLAMR RadCal

The nation's primary standard for optical power measurement or what the spectral power calibration is traceable to is the Primary Optical Watt Radiometer (POWR), an absolute cryogenic radiometer developed by NIST [20]. The uncertainties of its measurements are 0.01% (k = 1), which have been verified by an intercomparison with two other cryogenic radiometer facilities at NIST. POWR is installed adjacent to the NIST facility for SIRCUS, providing ready access to a variety of lasers. These lasers allow a broad range of wavelength and power levels to be selected for scale transfer to portable detectors, further reducing the uncertainties in the measurement chain. Additionally, the modularity of the critical detector section permits new POWR detector modules to be designed and built, which are better optimized for specific transfer wavelengths and power levels. The standard reference detectors, or the TRs, used for detector-based radiometric calibration are themselves calibrated directly against POWR using these tunable lasers as the source and establish radiometric scales in the visible–near-infrared region.

The GLAMR system currently has a total of fifteen radiometers to provide the absolute radiance output of the GLAMR integrating sphere. Five of these radiometers are silicon-based trap detector radiometers for the visible to NIR range; five are short-range single InGaAs detector radiometers for the spectral range less than 1600 nm; five are extended range InGaAs sphere-based detector radiometers for the spectral range longer than 1600 nm. The radiometers are used both within the GLAMR integrating sphere as Sphere Monitors (SMs) to provide an absolute measurement of the radiance during measurements, as well as externally to act as TRs between NIST and the sphere-based radiometers. These radiometers are periodically calibrated at NIST indirectly against POWR and then used to provide an absolute calibration for the object instrument by measuring radiance from the integrating sphere illuminated by GLAMR, the details of which are described in the next section. Figure 3 illustrates the traceability of the detector-based calibration to SI units using GLAMR. As is highlighted in the diagram, the critical component of the calibration is the GLAMR TR.

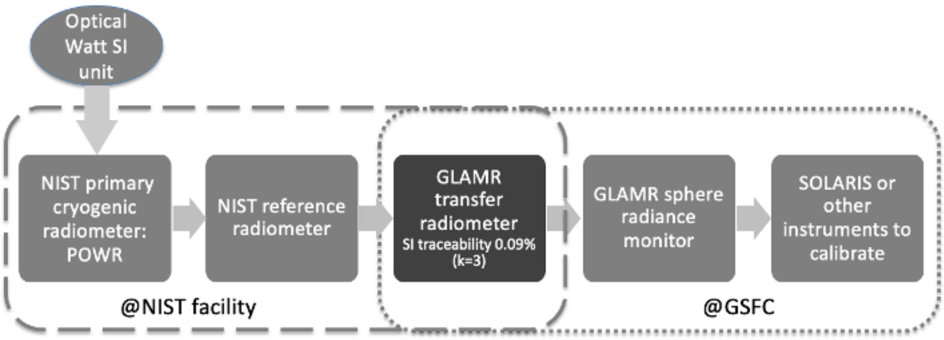

Figure 3. The traceability to SI units for the GLAMR radiometric calibration.

3. SOLARIS Absolute RadCal with GLAMR

3.1. SOLARIS Overview

SOLARIS is an Offner–Chrisp push-broom style imaging spectro-radiometer with a convex diamond-machined grating, covering a spectral region of 350–1000 nm. Its Focal Plane Array (FPA) is a 16-bit PCO pco.dege 5.5 CMOS camera of 2160 (spatial) $\times$ 2560 (spectral) detector elements (pixels). SOLARIS was designed and assembled at NASA GSFC as the calibration demonstration system for the RS instrument of the CLARREO mission. The similarities in the Offner-based design of SOLARIS to that of HySICS allow SOLARIS to be used as a surrogate system for HySICS in the development of the CPF independent calibration approach while moving forward the HySICS development without impacts to schedule. Component-level tests of the SOLARIS optics, detectors, grating, depolarizers, and attenuators have been performed. The characterized parameters are used as the inputs to the development of the SOLARIS instrument model.

3.2. Lab Setup for the SOLARIS RadCal

An optical fiber couples the GLAMR output to illuminate the integrating sphere used for sensor calibration. The three Sphere Monitors (SMs) are temperature-stabilized and permanently mounted to view the interior of the integrating sphere and provide the radiance from the integrating sphere. The relationship between the SMs and the exit port radiance is determined by placing the TRs in front of the exit port of the integrating sphere and comparing the SM and TR signals over the wavelength range of interest. The GLAMR team refers to this process as the Sphere Calibration. Figure 4 shows the positions of SMs and TRs along with the integrating sphere configured during a Sphere Calibration.

During the actual calibration, the sensor under test will replace the TRs in front of the integrating sphere.

Source tuning across the spectral ranges of the lasers is fully automated by computer control of the LBO temperature and tuning prism stages. This allows far higher data collection rates than would be possible with manual adjustment of the optics. Typical tuning increments are 30 s per wavelength, with 1 nm wavelength increments, although that can be modified depending on the test requirements. Several hundred calibration points can be obtained per day, and at a resolution of 1 nm, the entire spectral range of the OPO can be scanned over several days [12].

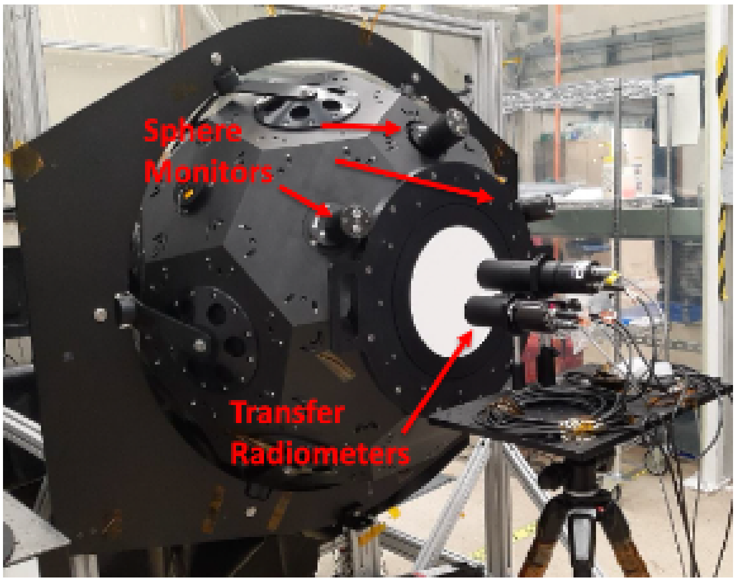

Figure 4. The lab setup for the Sphere Calibration to transfer the NIST calibration to the GLAMR sphere monitors. (Picture courtesy of the GLAMR team).

3.3. Data Collection

The data used in the current work were collected as part of a GLAMR absolute calibration of SOLARIS. SOLARIS was aligned to the exit port of the GLAMR integrating sphere to ensure full-field and full-aperture illumination. The Sphere Calibration took place shortly before the calibration. The collection timing is illustrated in Figure 5 [21]. The overall sequence is that the GLAMR source is tuned to a desired wavelength at which point a shutter is opened, illuminating the SMs and SOLARIS. The tuning process takes approximately 20 s, and the GLAMR shutter was opened for 30 s for the SOLARIS data collections. GLAMR telemetry data include wavelength as reported by a wave meter, SM output, shutter state, etc., that are collected at a 5 Hz frequency. Data sets are marked by the GLAMR Shutter (GS) states, as well as a wavelength step state number in order to identify the SOLARIS data corresponding to a given GLAMR tuning state.

One of the improvements that took place from the original GLAMR configurations is the inclusion of a time synchronization package that allows the data acquisition of the system under test to be synchronized with the clocks of the SM acquisition software and GLAMR's control software. The synchronization allows for easier matching of stabilized source signals with SOLARIS measurements. As a result, SOLARIS image acquisition is synchronized with GLAMR, but sampled at 1 Hz.

As described above, the GLAMR source is tuned through the full spectral range of the instrument with small steps in wavelength. Simultaneously, the GLAMR SMs provide the absolute radiance of the integrating sphere.

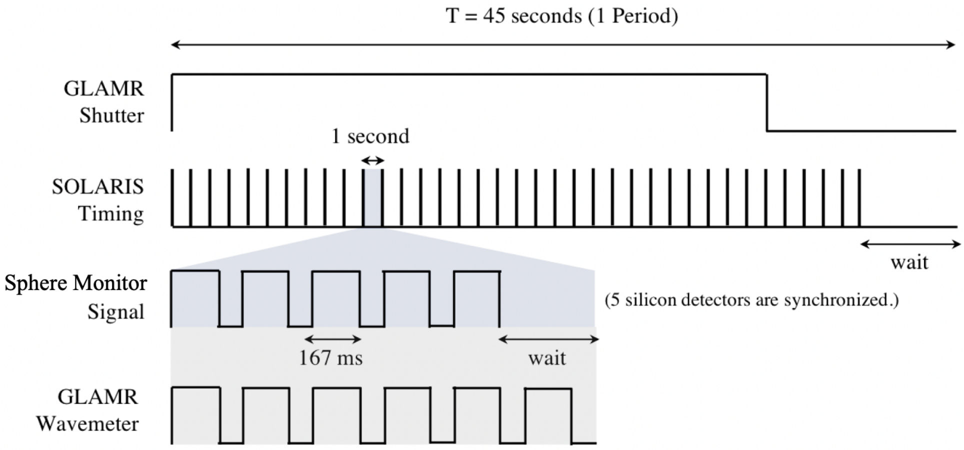

Figure 5. The time sequence of the data acquisition during SOLARIS GLAMR RadCal.

4. Data Processing and Results

4.1. SOLARIS RadCal Schedule

In the 2019 calibration, the entire responsivity range of the SOLARIS instrument from 350 nm to 1000 nm was scanned with 1 nm steps over 10 days over a three-month period. The test schedule is summarized in Table 2. Sampling strategies and testing dates were determined based on the availability of the GLAMR laboratory and personnel. Several spectral regions were repeated to evaluate spectral sampling effects. The scans from 560 nm to 675 nm, for example, were repeated with 0.5 nm wavelength steps. During measurements, one person operates the GLAMR source by tuning to prescribed wavelengths and radiance levels, while another operates the SMs and SOLARIS. On average, tuning GLAMR to the next increment and subsequent instrument measurements takes less than one minute.

Table 2. SOLARIS GLAMR RadCal schedule.

Date	Wavelength Range (nm)	$\Delta\lambda$ (nm)	Laser Type
7 March 2019	770–1000	1	NIR
8 March 2019	770–920	1	NIR
12 March 2019	385–568	1	NIR-SHG
13 March 2019	568–700	1	SWIR-SHG
14 March 2019	700–780	1	NIR
29 April 2019	378–470	1	NIR-SHG
30 April 2019	467–572	1	NIR-SHG
30 April 2019	778–1012	1	NIR
1 May 2019	560–779	1	SWIR-SHG
7 May 2019	560–675	0.5	SWIR-SHG
8 May 2019	560–675	0.5	NIR-SHG

4.2. GLAMR Data Processing

Due to the nature of laser tuning, the actual GLAMR wavelengths cannot match the setting values exactly. They are measured by the accompanying wave meter. The output of the SMs is converted to radiance using the NIST-based calibrations of the TRs through the Sphere Calibration. Quality checks of the GLAMR data are performed to remove data sets with invalid wavelengths. Valid SM data points are dark corrected based on data during the GLAMR shutter period and adjusted by the amplifier gain.

The dark-corrected and gain-adjusted SM signals s_{SM} are converted into radiance by

$$L(\lambda) = s_{SM} \cdot \frac{r_{TR}/r_{SM}}{g_{TR}}, \tag{1}$$

where the unit-less ratio between the TR signal and the SM signal r_{TR}/r_{SM} is derived from the Sphere Calibration, and the TR gain g_{TR} is calibrated at NIST. The processed GLAMR wavelength and radiance for 8 March 2019 are shown in Figure 6 for the OPO NIR laser as examples of typical output radiance levels for the SOLARIS calibration, as well as to show the wavelength sampling intervals. One key item to note in Figure 6b is that while the GLAMR system is tuned at a 1 nm sampling interval in this day, the actual wavelength steps vary noticeably. The fidelity of the automated tuning does not allow for exactly equal increments of wavelength sampling.

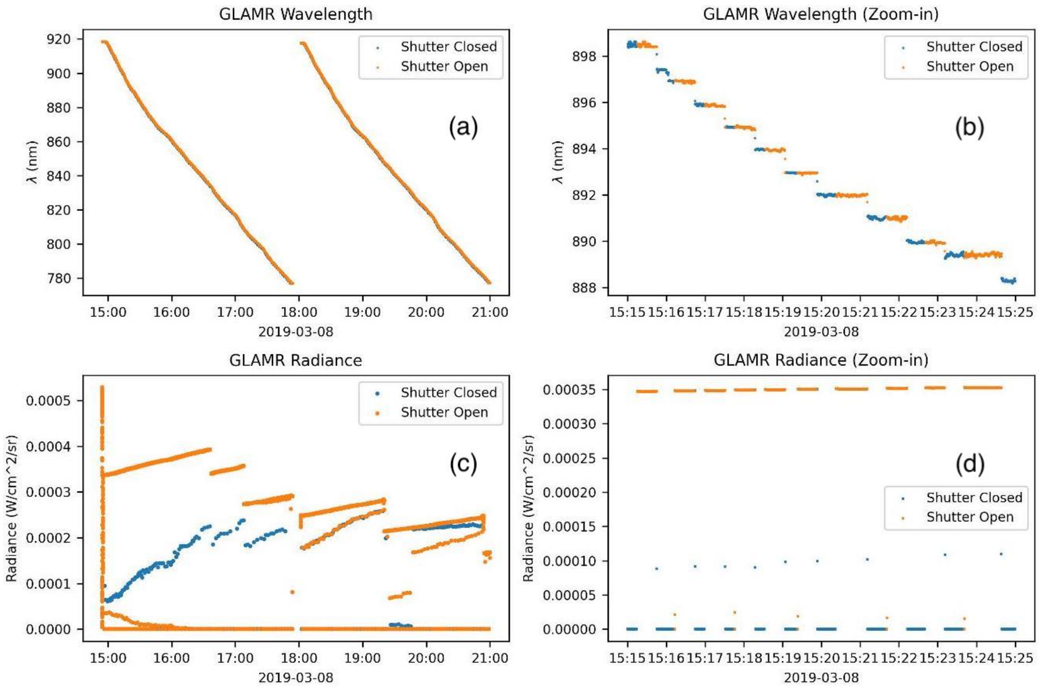

Figure 6. Outputs from the GLAMR monitors after pre-processing: (**a**,**b**) the wavelength; (**c**,**d**) the radiance. The input data are from 8 March 2019 measurements.

The variabilities of the GLAMR source wavelength and radiance are estimated and shown in Figure 7. The variability of the GLAMR wavelength and radiance during a SOLARIS measurement allows an assessment of the quality of the GLAMR data. Excessively large variability of either parameter indicates that the GLAMR system had not settled to a stable state, and thus, the SM value for the radiance would not be representative of the radiance seen by SOLARIS. Data points not meeting the quality metrics are repeated. Before integrating GLAMR data into the calculations, a moving average over collected data points in time is performed to reduce the operation frequency from 5 Hz to 1 Hz and apply filtering in measurement data to monitor unexpected changes. The average and standard deviations for the wavelength and radiance measurements were saved for the subsequent error analysis.

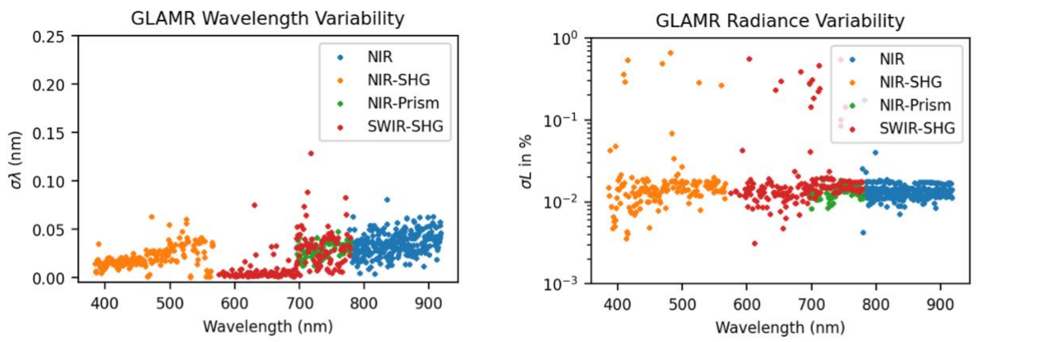

(**a**) (**b**)

Figure 7. The variability of GLAMR (**a**) wavelength and (**b**) radiance during 8 March 2019 measurements.

4.3. SOLARIS Data Processing

Of the 2160 spatial, or along the slit direction, samples of SOLARIS, Samples #3 to #2088, are illuminated by the GLAMR source. SOLARIS was operated without its order-sorting filter for the calibration, meaning that both the zeroth- and second-order light is present on the focal plane. The zeroth order is readily identified in the data since it is stationary at Spectral Pixel #229 independent of the wavelength. The range of GLAMR wavelengths is 378 to 1006 nm, which correspond to Spectral Columns #970 to #2166. The spectral mapping of wavelength to SOLARIS pixel number is nearly linear, with the fitting residue less than 0.5 nm for the whole spectral range, as is shown in Figure 8. The result indicates a well-designed and aligned spectrometer.

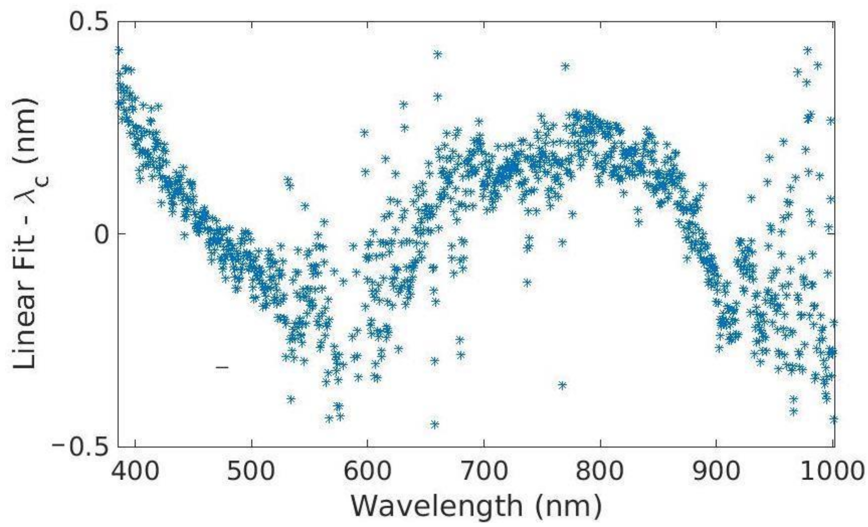

Figure 8. The residue of the center wavelength of SOLARIS spectral bands (pixels) from a linear mapping. The abscissa represents spectral bands denoted by their center wavelengths.

The initial SOLARIS data preparation includes a saturation check and dark subtraction. Each SOLARIS frame is checked to determine if the measured signal equals the bit depth, in which case the frame is discarded. Typically, SOLARIS acquired 30 "light" data frames at a particular GLAMR wavelength with 5 "dark" data frames with the shutter closed before and after the GLAMR measurement. The mean and standard deviation of the dark frames are stored in a 2160 $\times$ 2560 $\times$ 2 data cube with the first plane of the third dimension being the average and the second the standard deviation. The corresponding GLAMR data, wavelengths and radiance, are segmented based on the change in wavelength in order to identify the transition from one wavelength to another. GLAMR outliers are identified and removed using three scaled median absolute deviations, and the corresponding SOLARIS frames are culled. The peak location in the SOLARIS frames at a GLAMR wavelength is identified, and frames that deviated from the average location by more than twice the standard deviations are discarded. The mean and standard deviation of the SOLARIS data are calculated, and the resulting average frame is dark subtracted using a temporally proximate average dark frame. The Root Sum Square (RSS) of the dark-subtracted product is also calculated by the square root of the sum of squares assuming independence.

The reduced mean SOLARIS data at each wavelength are converted to the same time scale by dividing by the integration time of the acquisition. The data are accumulated into two cubes with dimensions 2086 (spatial) × 2560 (spectral) × 1281, where the last dimension corresponds to the different GLAMR wavelengths in ascending order. The first cube is in units of dark-subtracted Digital Numbers per second (DN/s). The second cube, referred to as the Absolute Spectral Response (ASR) cube, was divided by the appropriate GLAMR radiance value: for a given spectral detector (i,j), where i is the detector position in the spatial direction and j is the detector number in the spectral direction on the FPA, its ASR is calculated for each tuned GLAMR wavelength λ_k by

$$ASR_{\lambda_k} = \frac{\overline{S(\lambda_k)}}{L(\lambda_k)}, \quad (2)$$

where $S(\lambda_k)$ is the dark-corrected output of SOLARIS under test while viewing the GLAMR sphere source tuned to λ_k and $L(\lambda_k)$ is the GLAMR radiance for that wavelength as reported by the TRs with calibration by Equation (1). The resulting ASRs are in units of DN/s/(W/cm^{2}sr). The ∼30 image frames of $S(\lambda_k)$ captured at a tuned wavelength are averaged first before being used as the input of this ASR reconstruction. Figure 9 shows the reconstructed ASR for two arbitrarily selected spectral bands. Similarly, the standard deviation data were saved into two cubes. The GLAMR wavelength and radiance data are also stored in a separate data structure in ascending wavelength order.

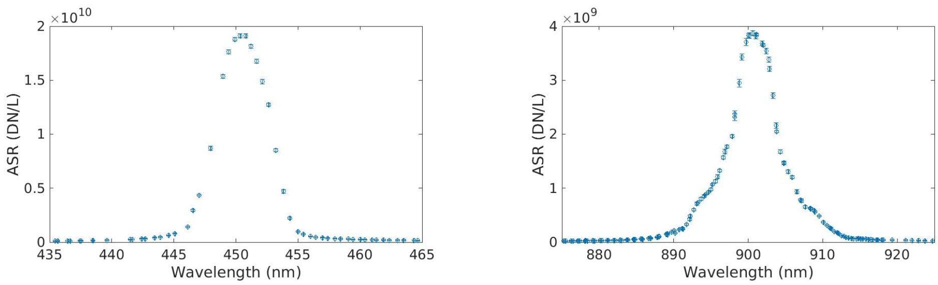

(**a**) (**b**)

Figure 9. Sample SOLARIS ASRs for (**a**) a visible band and (**b**) an NIR band.

In addition to data calibration, the characterization of the spectral response functions, or instrumental profiles in spectroscopy terminology, of an imaging spectrometer is critical to establish the instrument performance, in particular with regard to distortion control in the design and alignment of the instrument. For example, a poorly designed Offner–Chrisp will display some spatial–spectral non-uniformity with distortion being the primary field aberration that is manifest. This is often referred to as spectral smile [22]. For SOLARIS, the instrumental profiles were characterized with 1196 channel centers from 380.6 nm to 1001.3 nm for all 2160 of the spatial positions, enabling a robust evaluation of the imaging spectrometer quality.

The SOLARIS instrumental profiles have shoulders in particular at the longer wavelengths (see Figure 9b) and are not represented by an analytical function such as a Gaussian. This is partially due to the FPA used, which has a 6.5 µm pixel pitch. SOLARIS was designed for a pitch on the order of 20 µm with the typical root mean square spot radius around 15 µm, except at the longest wavelength and the widest field, where it reaches 21 µm (calculated from ray tracing). The design instrumental profiles, which are modeled as the convolution of the wider slit width, the target pixel pitch, and the line spread function, would have reduced shoulders compared with those measured here as the slit and pixel widths would be on the same order as the line spread function.

We addressed this asymmetry by fitting the data with a smoothing spline. This enables a robust evaluation of the instrumental profile center wavelengths and the Full-Width at Half-Maximum (FWHM). The center wavelength is defined as the location of the maximum splined ASR, not the band-averaged wavelength, because the former depends on the in-band response only and, thus, is more reliable when assessing all the bands across the whole spectral range. The variation in the center location is evaluated by taking the spatial average for each spectral channel, producing 1196 average centers and subtracting the appropriate average from each channel to produce a relative center value. Figure 10 illustrates a selection of the relative centers as a function of the spatial sample, and Figure 11 shows the average and standard deviation for all of the spectral channels on the left and the similar plot in the spectral direction on the right.

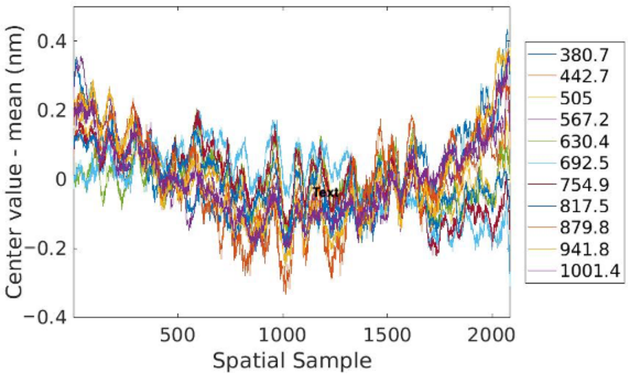

Figure 10. The relative center wavelengths as a function of spatial samples for 11 selected spectral columns.

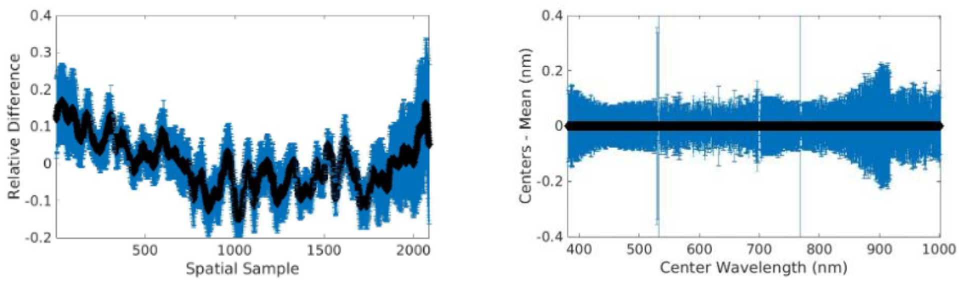

(**a**) (**b**)

Figure 11. The average and standard deviation of the relative center wavelengths for (**a**) all of the spectral channels per spatial sample and (**b**) all of the spatial samples per spectral channel denoted by the corresponding center wavelengths.

A similar analysis was performed to evaluate the uniformity of the FWHM of the instrumental profiles. The FWHMs are again determined from the smoothing spline fit. The relative FWHM is determined by averaging the FWHMs for all of the channels, yielding 5.7835 ± 0.0417 nm, and subtracting the mean from each spatial–spectral position. Figure 12 shows the results.

It is apparent that there is systematic variation in both the relative centers and relative widths. While identifying its exact root-cause may require an extensive investigation at component level that is unlikely to take place, we believe the variation is due to slight imperfections in the slit width.

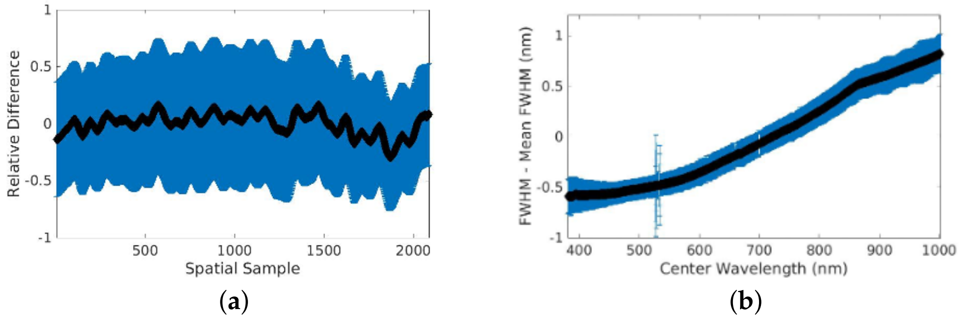

Figure 12. The relative FWHM for (**a**) all of the spectral channels per spatial sample and (**b**) all of the spatial samples per spectral channel denoted by the corresponding center wavelengths.

4.4. Characterization of Band Parameters

The resulting ASR can be used to further derive the Relative Spectral Response (RSR) and a number of parameters typically used to characterize a spectral band such as the band-integrated responsivity R_{BI}, Center Wavelength (CW) λ_{BA}, and Bandwidth (BW) or the FWHM. It is noted here that although the names of these parameters are associated with a band, they can be characterized at the detector level. For simplicity, the following results are restricted to detectors in one row along the spectral direction, and the spatial variation along the spatial direction is not further analyzed. Figure 13 shows the ASRs of a set of representative SOLARIS detectors after post-processing over the 350 to 940 nm wavelength range. In this figure and the following ones, the detector number j is projected to the CW of a detector to denote it for the convenience of the tracking.

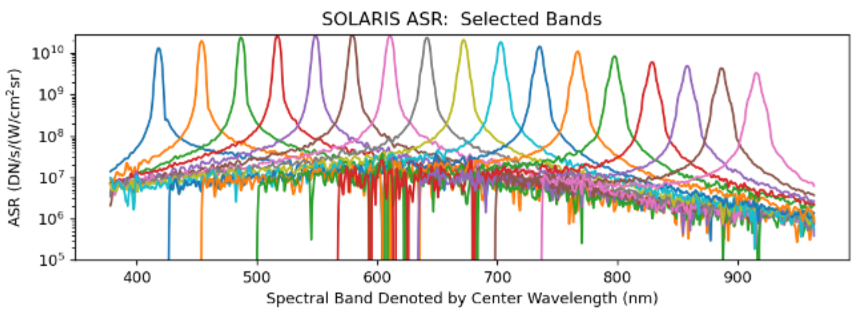

Figure 13. ASRs for representative SOLARIS spectral bands (detectors) after post-processing.

An ASR can be converted to a normalized RSR, a more traditional parameter measured to characterize the spectral variability of the detector response, via division by its peak value α:

$$RSR = \frac{ASR}{\alpha}. \tag{3}$$

To describe the radiometric property of a spectral detector, it is of greater interest to derive the gain of the detector to allow conversion of the detector output to a spectral radiance. The band-integrated responsivity R_{BI} can be computed from the ASR through a trapezoidal summation of the individual ASRs across the spectral region as [23]:

$$R_{BI} = \sum_{k=2}^{k_{max}} [\frac{ASR(\lambda_k) + ASR(\lambda_{k-1})}{2}][\lambda_k - \lambda_{k-1}], \tag{4}$$

where R_{BI} in units of DN·nm/s/(W/cm^{2}sr) is essentially the area below the ASR curve. Trapezoidal summation approximates the curve by using a piecewise linear connection of the ASR data points. Similarly, the curve can be approximated with piecewise constant values (mid-point rule) or quadratic functions (Simpson's rule). Implementing Equation (4) in calibration assumes that the incident laser energy is spectrally narrow enough to be considered monochromatic, and thus, the reconstructed ASR is a spectral ASR (λ_k). The response of the detector to any incident light is then the multiplication of R_{BI} and the band-averaged spectral radiance. Therefore, any error in R_{BI}'s calculation is propagated to the error of the radiometric calibration, making it a key bridging parameter for the error analysis of the GLAMR RadCal.

The band-averaged CW for a detector can also be calculated by trapezoidal summation as

$$\lambda_{BA} = \frac{\sum_{k=2}^{k_{max}} \lambda_k ASR(\lambda_k) + \lambda_{k-1} ASR(\lambda_{k-1})}{\sum_{k=2}^{k_{max}} ASR(\lambda_k) + ASR(\lambda_{k-1})}, \tag{5}$$

and the bandwidth can be calculated by

$$BW = \frac{1}{\alpha} \sum_{k=2}^{k_{max}} [\frac{ASR(\lambda_k) + ASR(\lambda_{k-1})}{2}][\lambda_k - \lambda_{k-1}]. \tag{6}$$

In Equations (5) to (6), the summations are across the whole wavelength regions from 350 to 940 nm, which include both the In-Band (IB) region, which can be defined between 1% of the peak responsivity, and the Out-Of-Band (OOB) region. Figure 14 shows the band-integrated responsivity, CW, and BW of the representative SOLARIS detectors. The summation can also be limited to the IB region alone. For a hyperspectral sensor like SOLARIS, the IB region is narrow, so the results of IB and OOB summations could differ noticeably due to the existence of detector read noise or other artifacts, as is shown in the figure. To emphasize this, the FWHMs of the spectral bands are calculated and overplotted with the BW, exhibiting a significantly reduced width.

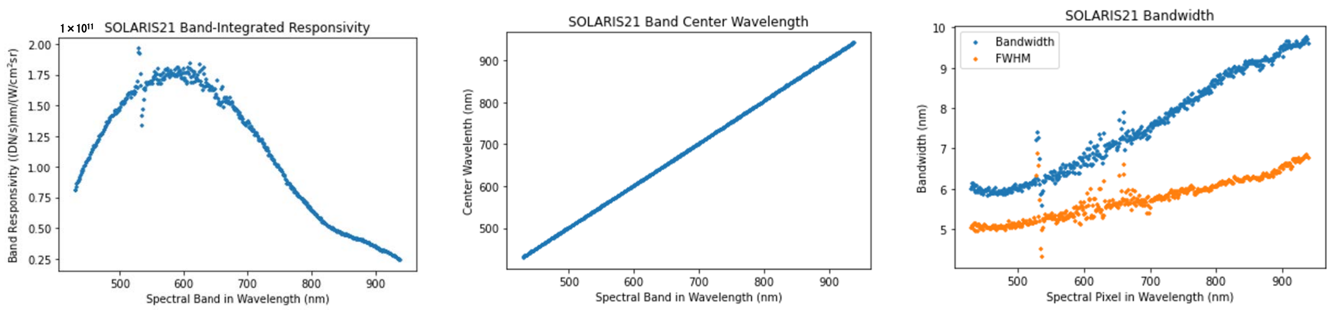

(**a**) (**b**) (**c**)

Figure 14. The characterized (**a**) band-integrated responsivity, (**b**) center wavelength, and (**c**) bandwidth & FWHM of SOLARIS bands (detectors).

While the trending of these parameters along the spectral direction is overall smooth, reflecting the smooth variation of the detector spectral response, outliers can be seen in certain regions such as 525–540 nm, which corresponds to the transition between NIR-SHG and SWIR-SHG lasers. The detector ASRs are then reconstructed from data with two laser sources at quite different magnitudes, and larger uncertainty is introduced in the aggregation and interpolation processes, in particular for those detectors whose IB responses lie within this region.

5. Discussion

5.1. Uncertainties

NIST's SIRCUS facility is the basis of the original GLAMR source and TRs and is the basis for the original error budget developed for the CLARREO reflected solar instrument [24]. That work showed that a prelaunch absolute radiometric calibration using a detector-based approach has two major uncertainties: (1) the GLAMR source and (2) uncertainties from the sensor under test. The first is primarily related to the absolute radiometric calibration of the detector standards, and the second is related to alignment, stray light, and the noise effects of the sensor being tested. The original work with SIRCUS indicated that the source uncertainty would be <0.2% (k = 2), which was more than sufficient to allow CLARREO to achieve its on-orbit 0.3% (k = 2) requirement.

Work with the GLAMR system on subsequent projects, including CPF, indicates that the current uncertainties are 0.6% (k = 2). Figure 15 shows the error terms for the radiance leaving the GLAMR integrating sphere from a former analysis [25]. The values here are estimated in collaboration with the SIRCUS developers at NIST. The sources of uncertainty include the variability of the GLAMR radiance and wavelength characterized in Figure 7, the non-uniformity of the integrating sphere, and the repeatability of the Sphere Calibration. It also includes the uncertainty of the NIST calibration of the TRs. The stated accuracy to calibrate TRs in irradiance mode using POWR is 0.09% (k = 3), and the accuracy of such a radiance-based calibration has been demonstrated in NIST facilities to an expected accuracy of 0.2% (k = 3).

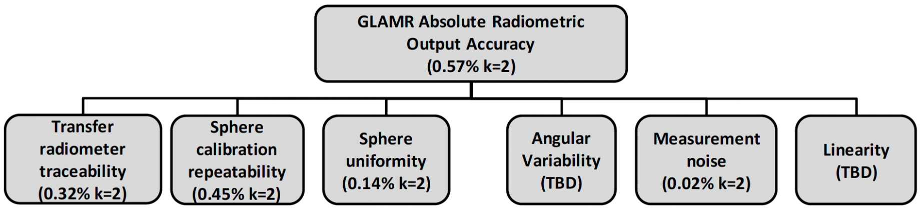

Figure 15. The proposed uncertainty budget of GLAMR RadCal on the entrance of a sensor under test. The values are representative of the values expected for the 400 to 950 nm spectral range.

The TRs traceability was estimated to be 0.09% (k = 3) in the original SIRCUS work [18], but additional tests of the TRs' stability, linearity, and current laboratory configuration set this value as 0.32% (k = 2) over the VNIR range of SOLARIS. Other studies as part of the update now show that uncertainties for TRs operating from 1100 to 1800 nm have values of 0.6% to 1.0% (k = 2) with larger uncertainties at longer wavelengths. Efforts are underway with NIST to reduce the uncertainties for the InGaAs detectors to a level similar to the silicon trap detectors. A portion of the uncertainty reported here is a result of changes in the response of the radiometers between NIST calibrations. The cause of the large changes and the temporal nature of the change are under investigation to decouple variation in TRs versus the absolute uncertainty of POWR and to determine if more frequent NIST characterizations will reduce this uncertainty.

An additional uncertainty that has increased significantly from earlier estimates is that related to the use of a sphere source to provide a radiance calibration as opposed to irradiance. It is well understood that the use of radiance leads to additional uncertainties, but the trade is that a radiance source is needed in order to ensure a proper calibration of the sensor in a configuration most like what will be encountered when in use. The early work assumed an effect due to the use of an extended source to add <0.2% (k = 2) to the TR uncertainty. Updated values have been obtained through the repeatability and uniformity studies of the integrating sphere including spheres more similar to those used for satellite sensor calibrations.

The integrating sphere repeatability uncertainty shown in Figure 15 is based on the variability of the Sphere Calibrations performed by the GLAMR team over time. The value in the figure is the 2σ standard deviation of the various calibrations that have been performed. The sphere calibrations include those performed without moving the integrating sphere from one location to another, as well as pre- and post-shipment collections. Thus, the 0.45% value is viewed as a conservative value since it includes cases for which real changes have occurred in the behavior of the integrating sphere that are properly taken into account when calibrating the test sensor. Sphere uniformity measurements made both by NIST and NASA indicate a realistic value of 0.14% (k = 2). These data were obtained by scanning a relatively narrow field of view non-imaging radiometer across the sphere ports to map the spatial variability. It is expected that the uncertainty for the SOLARIS case will be smaller since the GLAMR integrating sphere is out of focus during the SOLARIS calibration, but the 0.14% value is used as a conservative value for this work.

The remaining three uncertainties are much smaller than the first three. The angular variability is a result of the fact that the sensor under test and TRs measure the sphere normal to the exit port, while the monitoring radiometers view non-normal. The uncertainty from this error source is still being quantified for the SOLARIS test data, but is expected to be <<0.1% based on studies using the spatial uniformity data sets. The signal variation is the result of noise in the the TRs. The 2σ variation of long-term collections performed as part of the SOLARIS work with the GLAMR source held stable in wavelength and radiance over several minute time periods provide the 0.02% (k = 2) value given. The last error source given is the effect caused by the non-linearities of the TR and SM responses. Evaluations by NIST have shown these radiometers to have non-linearity uncertainties <0.01% over several decades of signal. Work is currently underway to quantify this effect for the GLAMR TRs and SMs, but since the SOLARIS results here did not approach the upper end of the SM response, the uncertainty is considered to be negligible for the results here.

The overall uncertainty of the GLAMR calibration of SOLARIS also includes uncertainties caused by the SOLARIS system, as well as its interaction with the GLAMR integrating sphere. A portion of this latter uncertainty is carried in the sphere uniformity uncertainty shown in Figure 15. Other effects include possible vignetting and integrating sphere loading from back reflections of the SOLARIS system with the GLAMR integrating sphere. Both of those have been studied by the GLAMR team during past calibrations of other sensors and have shown that the uncertainties are <0.1%. The effects from the SOLARIS sensor itself are discussed in Sections 5.2 and 5.3.

5.2. Repeatability

Assessing the absolute uncertainties for the SOLARIS calibration requires an assessment of the sensor's impact on the calibration. One method to evaluate this uncertainty is through the repeatability of the SOLARIS calibration from the multiple GLAMR calibrations performed over the 780 nm to 920 nm spectral region.

Figure 16 shows the processed telemetry data from GLAMR as a function of the tuned GLAMR wavelength. The telemetry data were averaged at 30 s intervals to represent the approximate temporal duration during SOLARIS collections at a GLAMR-tuned wavelength. The figure shows the percent standard deviation of the average GLAMR reported wavelength and radiance. Indicated on the graphs also are the GLAMR-based uncertainties provided in the previous section.

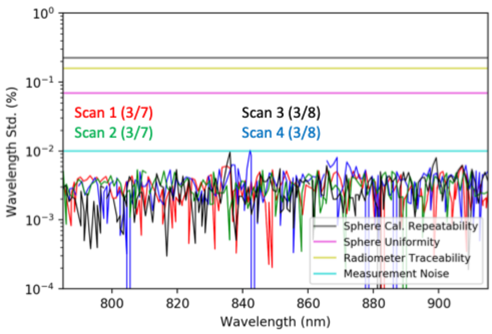

(**a**)

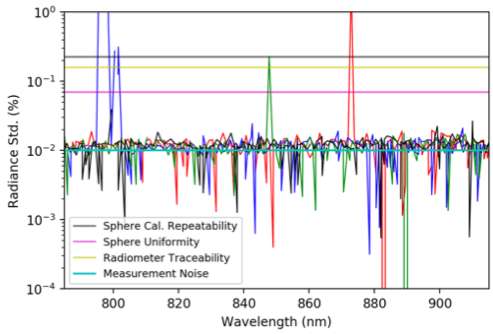

(**b**)

Figure 16. Processed GLAMR telemetry results from four scans collected over the 780–920 nm spectral range: (**a**) the variability of GLAMR wavelength and (**b**) the variability of GLAMR radiance.

The results indicate that the wavelength variability is very similar for all four collections and is small in magnitude. One area that is still currently under evaluation is how best to convert an uncertainty in wavelength to that of an uncertainty in the source radiance at a given wavelength to be coupled into the radiance uncertainty budget. The challenge is that the GLAMR approach to calibration means that there is not a well-behaved change in radiance as a function of wavelength as is typical for most broadband, blackbody sources such as halogen lamps. The work here assumes that the variation in response of the SMs is negligible over the variability of the wavelength and that the radiance can be assumed to be constant over a change in wavelength.

The radiance results in Figure 16 from the four collects behave in a similar fashion with similar variability across all four. The magnitude of the variability is of the same order as the sphere monitor measurement noise uncertainty, indicating that this uncertainty is well understood. It is noted that there are multiple wavelengths for which the radiance standard deviation far exceeds the measurement noise uncertainty. Such behavior is typically caused by the GLAMR source, requiring longer time periods to settle to a stable radiance value at a tuned wavelength. It is clear that these effects are not repeatable, both over specific wavelength regions and across the multiple collections. It has been found that the GLAMR calibration efficiency is improved by allowing the system to tune through the full spectral range in an automated fashion and then to go back and manually tune the system to repeat those data points with excessive measurement noise.

The GLAMR calibration data from the four collections were processed to band-integrated responsivity R_{BI} by Equation (4). It is recognized that these data ignore the OOB region of the response, but the goal of the multiple collections was to evaluate calibration repeatability. The OOB effects are minimized by examining the repeatability of the band-averaged spectral response for bands between 800 and 890 nm. Figure 17 shows the retrieved responsivity values and the difference between a given calibration value and the mean of all four collections. The standard deviation of the mean does not show a strong wavelength dependence with a value of 1.5%. It is clear that the variation in R_{BI} is much larger than that of the absolute uncertainty described in the previous section.

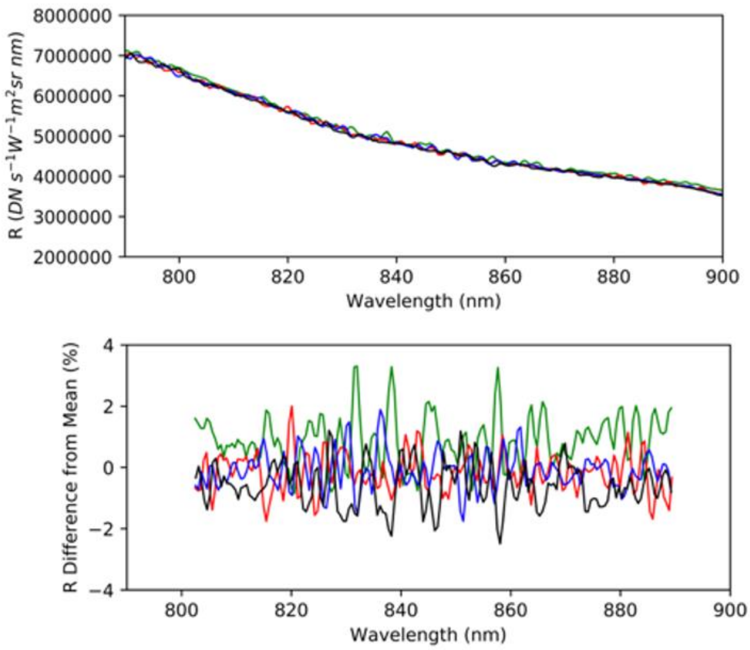

Figure 17. The SOLARIS gain results based on four individual spectral scans from 780 nm to 920 nm with GLAMR.

The variability of the SOLARIS band-averaged spectral response can be caused by uncertainties in the GLAMR radiance, GLAMR wavelength, and SOLARIS instrument variability. The GLAMR telemetry data show that the GLAMR source is an unlikely cause of the response variation over the four calibrations. Examination of the SOLARIS raw signal variation at a given tuned GLAMR wavelength shows an order of magnitude larger than the telemetry variations. Verification of the effect being due to SOLARIS sensor behavior has been obtained by comparisons with GLAMR calibration data from a multispectral field transfer radiometer that is being used as a high SNR instrument with high radiometric stability to evaluate the absolute uncertainties of surface reflectance field measurements [26].

The multispectral instrument was operated in tandem with SOLARIS for one of the calibration collections with GLAMR for a single band of the multispectral system. A representative result is shown in Figure 18 giving the digital output in DN/s for both instruments at a single tuned GLAMR wavelength. More details about the instrument and the experiment are provided in Section 5.3. The DN/s data were normalized to the peak value for both sensors. The mean of the SOLARIS data is also shown on the graph. The results clearly show that the SOLARIS instrument variability is much larger than that of the multi-spectral system. Current data analysis indicates that the variability is related to the low SNR for the SOLARIS data, both from integration time and numbers of frames collected, as well as due to low radiance levels from GLAMR [27].

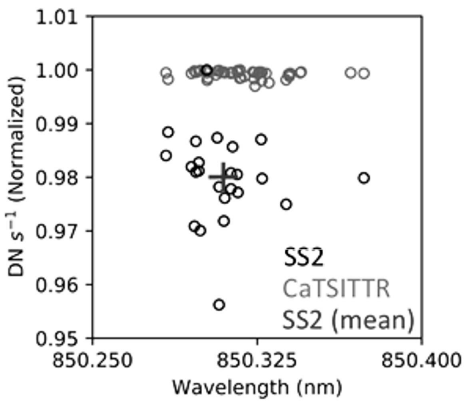

Figure 18. Comparison of relative Digital Numbers (DNs) between the multispectral system (labeled CaTSSITTR; more details about the instrument are provided in Section 5.3) and the SOLARIS data (labeled SS2) for a single GLAMR-tuned wavelength. The mean values of the SOLARIS data are shown by the + sign.

The SNR, integration time, and number of frames are being evaluated to determine optimal configurations for future calibrations of SOLARIS with GLAMR. Schedule and laboratory availability have not allowed for follow-up calibration work at the time of the writing of this manuscript. An additional factor that plays a role in the repeatability of the GLAMR-based calibration is the spectral sampling of the calibration. Analysis of portions of the SOLARIS results for which there is better repeatability indicate that an SNR >200 combined with 30 SOLARIS frames and a GLAMR sampling of 1 nm will ensure that the GLAMR source is the limiting uncertainty in the absolute error budget.

5.3. Multi-Spectral Source-Based Results

The results shown in Section 5.2 indicate that SOLARIS SNR of the GLAMR calibration limits the ability to validate the absolute uncertainty budget. Attempts were made early in the SOLARIS work to have source-based absolute calibrations [24], but changes in the SOLARIS focal plane and subsequent budget and schedule limitations have prevented the opportunity for a detector-based comparison to source-based results. The multispectral radiometer mentioned in Section 5.2 is used here to help validate the absolute uncertainty of the GLAMR-based calibration. Such a validation is admittedly a challenge since the lowest uncertainty, source-based calibration is still twice the GLAMR-based absolute uncertainty shown above.

The Calibration Test Site SI-Traceable Transfer Radiometer (CaTSSITTR) is a small portable transfer radiometer that acts as a traveling transfer standard for vicarious calibration [28]. The radiometer's design emphasized portability while not sacrificing radiometric stability. The absolute source-based calibration of CaTSSITTR was performed multiple times during the time period including a GLAMR-based calibration of the radiometer at the Remote Sensing Group's radiometric calibration facility at the University of Arizona [29]. The most accurate source-based method from that facility is one in which a NIST-supplied FEL lamp illuminates a NIST-calibrated diffuser plaque. The geometry of the measurements is well controlled, as is the lamp operation. The absolute uncertainties of the source-based calibration have recently been evaluated to be 1.4% ($k = 2$) at 900 nm and 1.6% ($k = 2$) at 550 nm [29].

Figure 19 shows the percent difference between GLAMR-based absolute radiometric calibration of the multispectral field transfer radiometer and the lamp–plaque source-based approach (solid line). The data collection and processing of the GLAMR calibration follows the method described above. The error bars shown for the lamp–plaque results indicate the combined $k = 2$ uncertainty of the source- and detector-based methods. The encouraging result is that the agreement between GLAMR and the more traditional calibration approach is well within the combined uncertainties for wavelengths between 400 and 550 nm. Results at longer wavelengths differ by more than the combined uncertainties at a 95% confidence, indicating that the uncertainties of one of the approaches is not correct or there is an effect in the radiometer related to the different calibration approaches.

Initial evaluations of the radiometer do not indicate a clear cause of the larger-than-expected differences between the GLAMR and lamp results. Additional calibration methods have been used with the radiometer including a small-sized lamp-illuminated integrating sphere and a solar-illuminated plaque method. The sphere-based results have similar uncertainties to the lamp–plaque method, but have an independent calibration path. There is very good agreement between the sphere results and both GLAMR and lamp–plaque for the 400–550 nm spectral range. The sphere and plaque approaches also match each other well at 650 nm though diverging some at longer wavelengths, but are still within the combined $k = 2$ uncertainties of the approaches.

The solar-based approach has the advantage of relying on a significantly different spectral source from the lamp methods with similar uncertainties to the lamp-based methods, except in the blue portion of the spectrum due to atmospheric effects. The results shown here are an average of eight separate data sets collected over a range of solar zenith and atmospheric conditions. The solar-based results agree with GLAMR to better than the $k = 2$ combined uncertainties, as shown by the error bars in the figure, except for the longest radiometer wavelength. The solar-based approach agrees to within the $k = 2$ combined uncertainties of both lamp-based methods.

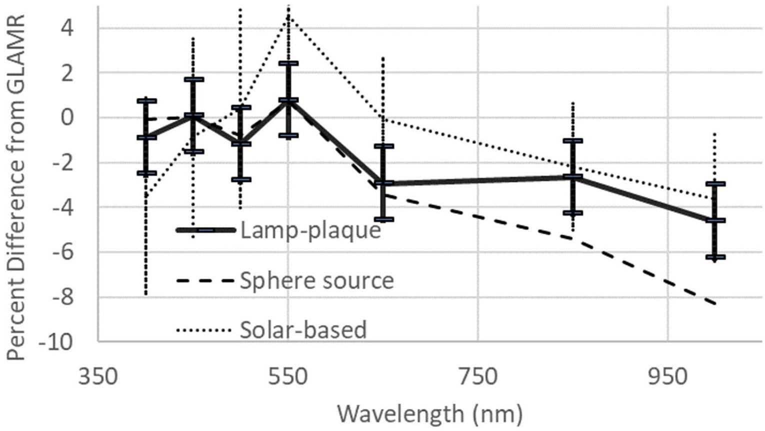

Figure 19. Percent difference between GLAMR-based absolute radiometric calibration of the multispectral field transfer radiometer and the lamp–plaque source-based approach (solid line). Error bars indicate the combined k = 2 uncertainty of the source- and detector-based methods. Shown for reference also are sphere-based and source-based results with combined uncertainty error bars shown for the solar-based method (sphere-based are similar to those of lamp–plaque).

Thus, it is not clear at this point what the cause of the distinct difference in behavior as a function of wavelength is. It should be noted that a repeat GLAMR calibration of the 850 nm band of the radiometer agreed with the original calibration to better than 0.4%. Multiple lamp–plaque measurements with multiple lamps and multiple dates have shown larger variability at longer wavelengths than would be expected. Planned efforts to evaluate the error budgets of the various approaches will include multiple other instruments, as well as lamp-based and solar-based calibrations of SOLARIS when time permits. The current results do, however, show that the SOLARIS calibration with GLAMR is as accurate as the lamp-based approaches, and there are indications that the current GLAMR absolute radiometer calibration error budget is valid.

6. Conclusions

A detector-based, absolute radiometric calibration of an imaging spectrometer using the GLAMR system was presented. The method used here relies on a tunable laser system to illuminate a sphere source that provides a full-field, full-aperture radiance calibration of the sensor under test. Tuning the laser source through the full spectral range of the test sensor provides the necessary data for both in-band and OOB response, providing quantitative stray light and ASR data. The extended source nature of the integrating sphere allows the spectral response to be determined for every detector in an imaging spectrometer.

The GLAMR calibration approach was applied to the SOLARIS instrument, which is the calibration demonstration system for the CLARREO Pathfinder project. The results showed that SOLARIS's Offner–Chrisp design combined with the optical alignment of the system minimizes spectral smile to <0.2 nm across the full field of view of the sensor for all spectral channels. Examination of the center wavelength derived for each detector showed small repeatable features, indicating effects from the slit. The ASRs showed effects caused by the choice of pixel pitch in the replacement focal plane not being well matched to the spectrometer point spread function. The end result is that the SOLARIS calibration shows the potential of a detector-based calibration of an imaging spectrometer.

The full potential of a GLAMR-based calibration will be achieved if the climate quality accuracies can be obtained. The dominant calibration uncertainty for the SOLARIS case has been shown to be due to SOLARIS noise effects resulting from GLAMR source radiance levels coupled with less-than-optimal integration times and SOLARIS samples. Indications are that an SNR > 200 combined with 30 SOLARIS frames and a GLAMR sampling at 1 nm are needed to ensure that the GLAMR source is the limiting uncertainty in the absolute error budget. These values were studied further as part of a sensitivity study to examine the impact of these parameters on the repeatability of retrieved band-averaged spectral response [27].

The results obtained in this work are being used to help define test protocols for the HySICS sensor for CPF independent calibration testing and can be extended further to other imaging spectrometers. The SOLARIS calibration combined with that of a multi-spectral radiometer using both source- and detector-based calibrations demonstrate that the GLAMR test setup already delivers an absolute radiometric accuracy that is no worse than current source-based approaches, and the lessons learned here can provide accuracies sufficient for the CPF independent calibration.

Author Contributions: Conceptualization and methodology, Z.W. and R.L.; software and formal analysis, Z.W., R.L. and K.T.; writing—original draft preparation, Z.W., R.L., K.T. and B.N.W.; writing—review and editing, Z.W., B.N.W., K.T. and R.L.; visualization, Z.W. and B.N.W.; supervision, project administration and funding acquisition, K.T. All authors have read and agreed to the published version of the manuscript.

Funding: The work shown here was supported by funds provided by the CLARREO Pathfinder Project.

Data Availability Statement: The data presented in this study are available on request from the corresponding author. The data are not publicly available due to their limited application.

Acknowledgments: The authors acknowledge the efforts and dedication of the NASA/GSFC GLAMR team for the development and operation of the GLAMR system and their support in the collection of the data used in this manuscript.

Conflicts of Interest: The authors declare no conflict of interest.

References

1. Cao, C.; Luccia, F.J.D.; Xiong, X.; Wolfe, R.; Weng, F. Early on-orbit performance of the Visible Infrared Imaging Radiometer Suite onboard the Suomi National Polar-Orbiting Partnership (S-NPP) satellite. *IEEE Trans. Geosci. Remote Sens.* **2014**, *52*, 1142–1156. [CrossRef]
2. Thome, K.J.; Helder, D.L.; Aaron, D.; Dewald, J.D. Landsat-5 TM and Landsat-7 ETM+ absolute radiometric calibration using the reflectance-based method. *IEEE Trans. Geosci. Remote Sens.* **2004**, *42*, 2777–2784. [CrossRef]
3. Xiong, X.; Butler, J.; Chiang, K.; Efremova, B.; Fulbright, J.; Lei, N.; McIntire, J.; Oudrari, H.; Sun, J.; Wang, Z.; et al. VIIRS on-orbit calibration methodology and performance. *J. Geophys. Res. Atmos.* **2013**, *119*, 5065–5078. [CrossRef]
4. Cao, C.; Xiong, J.; Blonski, S.; Liu, Q.; Uprety, S.; Shao, X.; Bai, Y.; Weng, F. Suomi NPP VIIRS sensor data record verification, validation, and long-term performance monitoring. *J. Geophys. Res. Atmos.* **2013**, *118*, 11664–11678. [CrossRef]
5. Wielicki, B.A.; Young, D.F.; Mlynczak, M.G.; Thome, K.J.; Leroy, S.; Corliss, J. Achieving climate change absolute accuracy in orbit. *Bull. Am. Meteorol. Soc.* **2013**, *94*, 1519–1539. [CrossRef]
6. CLARREO Pathfinder Mission. Available online: https://clarreo-pathfinder.larc.nasa.gov/ (accessed on 22 February 2022).
7. TRUTHS Satellite Calibration Mission. Available online: https://www.esa.int/Applications/Observing_the_Earth/TRUTHS (accessed on 22 February 2022).
8. Lukashin, C.; Wielicki, B.A.; Young, D.F.; Thome, K.; Jin, Z.; Sun, W. Uncertainty estimates for imager reference inter-calibration with CLARREO reflected solar spectrometer. *IEEE Trans. Geosci. Remote Sens.* **2013**, *51*, 1425–1436. [CrossRef]
9. Kopp, G.; Smith, P.; Belting, C.; Castleman, Z.; Drake, G.; Espejo, J.; Heuerman, K.; Lanzi, J.; Stuchlik, D. Radiometric flight results from the HyperSpectral Imager for Climate Science (HySICS). *Geosci. Instrum. Method. Data Syst.* **2017**, *6*, 169–191. [CrossRef]
10. Woodward, J.T.; Shaw, P.S.; Yoon, H.W.; Zong, Y.; Brown, S.W.; Lykke, K.R. Invited Article: Advances in tunable laser-based radiometric calibration applications at the National Institute of Standards and Technology, USA. *Rev. Sci. Instrum.* **2016**, *89*, 091301. [CrossRef] [PubMed]
11. McIntire, J.; Moyer, D.; Brown, S.W.; Lykke, K.R.; Waluschka, E.; Oudrari, H.; Xiong, X. Monochromatic measurements of the JPSS-1 VIIRS polarization sensitivity. *Appl. Opt.* **2016**, *55*, 7444–7454. [CrossRef] [PubMed]
12. McAndrew, B.; McCorkel, J.; Shuman, T.; Zukowski, B.; Traore, A.; Rodriguez, M.; Brown, S.; Woodward, J. Goddard laser for absolute measurement of radiance for instrument calibration in the ultraviolet to short wave infrared. In Proceedings of the Conference on Lasers and Electro-Optics (CLEO), San Jose, CA, USA, 5–10 May 2018; pp. 1–2.
13. Barsi, J.A.; McCorkel, J.; McAndrew, B.; Zukowski, B.; Shuman, T.; Johnston, S.; Markham, B. Spectral testing of the Landsat-9 OLI-2 instrument using the Goddard Laser Absolute Measurement of Radiance (GLAMR). In *Earth Observing Systems XXIII*; International Society for Optics and Photonics: Bellingham, WA, USA, 2018; Volume 10764, p. 1076405.
14. Angal, A.; McCorkel, J.; Thome, K. Evaluation of GLAMR-based calibration for SI-traceable field reflectance retrievals. In *Earth Observing Systems XXI*; SPIE: Bellingham, WA, USA, 2016; Volume 9972, p. 99721U.

15. International Vocabulary of Metrology—Basic and General Concepts and Associated Terms (VIM), 3rd ed. 2006. Available online: https://www.nist.gov/system/files/documents/pml/div688/grp40/International-Vocabulary-of-Metrology.pdf (accessed on 22 February 2022).
16. Wyatt, C. *Radiometric Calibration: Theory and Methods*, 1st ed.; Elsevier: Amsterdam, The Netherlands, 1978. [CrossRef]
17. Thome, K.; Markham, B.; Barker, J.; Slater, P.; Biggar, S. Radiometric calibration of Landsat. *Opt. Sci.* **1997**, *63*, 853–858.
18. Brown, S.W.; Eppeldauer, G.P.; Lykke, K.R. Facility for spectral irradiance and radiance responsivity calibrations using uniform sources. *Appl. Opt.* **2006**, *45*, 8218–8237. [CrossRef] [PubMed]
19. McAndrew, B. Goddard Laser for Absolute Measurement of Radiance. In Proceedings of the Surface Biology and Geology Community Workshop, Washington, DC, USA, 12–14 October 2019.
20. Houston, J.M.; Rice, J.P. NIST reference cryogenic radiometer designed for versatile performance. *Metrologia* **2006**, *43*, S31–S35. [CrossRef]
21. Aytac, Y.; Thome, K.; Wenny, B.N.; Angal, A.; Shuman, T.M.; McAndrew, B. Detector based calibration of a portable imaging spectrometer for CLARREO Pathfinder mission. In *Earth Observing Systems XXIV*; International Society for Optics and Photonics: Bellingham, WA, USA, 2019, Volume 11127, p. 111270A. [CrossRef]
22. Folkman, M.A.; Pearlman, J.; Liao, L.B.; Jarecke, P.J. EO-1 Hyperion hyperspectral imager design, development, characterization, and calibration. *Hyperspectral Remote. Sens. Land Atmos.* **2001**, *4151*, 40–51. [CrossRef]
23. Barnes, R.A.; Brown, S.W.; Lykke, K.R.; Guenther, B.; Butler, J.J.; Schwarting, T.; Turpie, K.; Moyer, D.; DeLuccia, F.; Moeller, C. Comparison of two methodologies for calibrating satellite instruments in the visible and near-infraed. *Appl. Opt.* **2015**, *54*, 10376–10396. [CrossRef] [PubMed]
24. Thome, K.; McCorkel, J.; McAndrew, B. Demonstrating the error budget for the Climate Absolute Radiance and Refractivity Observatory through solar irradiance measurements. In *Earth Observing Systems XX*; International Society for Optics and Photonics: Bellingham, WA, USA, 2015; Volume 9607, p. 96071C. [CrossRef]
25. Thome, K.; Aytac, Y. Independent calibration approach for the CLARREO Pathfinder Mission. In *Imaging Spectrometry XXIII: Applications, Sensors, and Processing*; International Society for Optics and Photonics: Bellingham, WA, USA, 2019; Volume 11130, p. 111300B. [CrossRef]
26. Thome, K.; Wenny, B.; Anderson, N.; McCorkel, J.; Czapla-Myers, J.; Biggar, S. Ultra-portable field transfer radiometer for vicarious calibration of earth imaging sensors. *Metrologia* **2018**, *55*, S104–S107. [CrossRef] [PubMed]
27. Salehi, F.; Thome, K.; Wenny, B.N.; Lockwood, R.; Wang, Z. Band averaged response sensitivity study of an imaging spectrometer for CLARREO Pathfinder mission. *Remote Sens.* **2022**, *submitted*.
28. Anderson, N.; Thome, K.; Czapla-Myers, J.; Biggar, S. Design of an ultra-portable field transfer radiometer supporting automated vicarious calibration. In *Earth Observing Systems XX*; SPIE: Bellingham, WA, USA, 2015; Volume 9607, p. 960709.
29. Thome, K.; Czapla-Myers, J.; Wenny, B.; Andersonr, N. Calibration and use of an ultra-portable field transfer radiometer for automated vicarious calibration. In *Earth Observing Systems XXII*; International Society for Optics and Photonics: Bellingham, WA, USA, 2017; Volume 10402, p. 104020L.